

# Investigation of the spall strength of graphite using nano- and picosecond laser pulses

I K Krasnyuk<sup>1</sup>, A Yu Semenov<sup>1</sup>, I A Stuchebryukhov<sup>1</sup>, R S Belikov<sup>2</sup>,  
K V Khishchenko<sup>2</sup>, O N Rosmej<sup>3</sup>, T Rienecker<sup>3</sup>, A Schoenlein<sup>4</sup> and  
M Tomut<sup>5</sup>

<sup>1</sup> Prokhorov General Physics Institute of the Russian Academy of Sciences, Vavilova 38,  
Moscow 119991, Russia

<sup>2</sup> Joint Institute for High Temperatures of the Russian Academy of Sciences, Izhorskaya 13  
Bldg 2, Moscow 125412, Russia

<sup>3</sup> GSI Helmholtzzentrum für Schwerionenforschung GmbH, Planckstraße 1, Darmstadt 64291,  
Germany

<sup>4</sup> Goethe University Frankfurt am Main, Grüneburgplatz 1, Frankfurt am Main 60323,  
Germany

<sup>5</sup> Technical University Darmstadt, Karolinenplatz 5, Darmstadt 64289, Germany

E-mail: [krasnyuk99@rambler.ru](mailto:krasnyuk99@rambler.ru)

**Abstract.** Spallation phenomena in graphite targets were investigated experimentally under nano- and picosecond shock-wave action at laser facilities “Kamerton-T” (GPI RAS) and PHELIX (GSI). In the range of strain rates of 1 to 10  $\mu\text{s}^{-1}$  at the first time, data of dynamic tensile strength of the material were obtained. At maximal realized strain rate of 14  $\mu\text{s}^{-1}$ , the spall strength value 2.1 GPa has been achieved that is 64% of the theoretical ultimate tensile strength of the graphite. Spallation was observed not only on the backside of the target, but also on its front (irradiated) surface. The morphology of the front and rear surfaces of the targets was studied using the optical and scanning electron microscopy. The structure of the graphite in irradiated area on the facial side as well as in the spallation zone on the rear side of the target was investigated by Raman scattering method. A comparison of the dynamic strength of the graphite with the dynamic strength of a synthetic diamond is done.

## 1. Introduction

In this paper, some results of experimental-theoretical study of peculiarities of the spallation phenomenon in graphite samples are presented. For generating a tensile stress (negative pressure), the samples were subjected to shock-wave action of laser pulses of 1.4-ns duration at PHELIX laser facility (GSI, Darmstadt, Germany) and 70-ps duration at “Kamerton-T” laser system (GPI, Moscow, Russia). In both cases, the wavelength of the laser beam was 0.53  $\mu\text{m}$ .

The spallation phenomenon [1] arises near the back (free) surface of a target after arrival of a compression wave, which is generated (in the case) by pulsed laser irradiation of the front (facial) surface of the target. Because of smallness of backpressure on the free surface, the matter accelerated in the shock wave takes an additional acceleration that causes a propagation of a rarefaction wave towards the compression pulse and successive rarefaction wave from the facial surface. At some distance from the back surface, the pressure in the target becomes negative,



**Table 1.** Experimental details:  $D_{\text{inp}}$ —diameter of the focal spot,  $E_l$ —laser pulse energy,  $I_l$ —laser intensity in the focal spot on the target,  $P_a$ —ablation pressure,  $D_{\text{sp}}$ —diameter of the spallation region,  $H_0$ —target thickness,  $h_{\text{sp}}$ —spall plate thickness,  $\tau$  and  $\lambda$ —duration and wavelength of the laser radiation, respectively.

Sample No.	$D_{\text{inp}}$ , mm	$E_l$ , J	$I_l$ , TW/cm <sup>2</sup>	$P_a$ , TPa	$D_{\text{sp}}$ , mm	$H_0$ , $\mu\text{m}$	$h_{\text{sp}}$ , $\mu\text{m}$
Graphite MF-307, “Kamerton-T”, $\tau = 70$ ps, $\lambda = 0.53$ $\mu\text{m}$							
1	0.343	0.748	11.0	0.41	0.343	220	65
2	0.370	0.941	11.5	0.43	0.411	220	70
3	0.288	0.826	16.0	0.55	0.320	410	175
Graphite PG-5, PHELIX, $\tau = 1.4$ ns, $\lambda = 0.53$ $\mu\text{m}$							
4	3.70	122	2.1	0.13	3.1	2100	400
5	1.35	120	6.0	0.28	3.5	2000	200
6	1.35	107	5.4	0.26	2.87	1100	80

at that the tensile stress may exceed the spall (tensile) strength of the material. That leads to spallation of some layer from the initial sample.

In our experiments, samples of polycrystalline graphite MF-307 (density 2 g/cm<sup>3</sup>), and PG-5 (density 1.84 g/cm<sup>3</sup>) were used.

The value of theoretical ultimate tensile strength of a material  $\sigma_{\text{th}}$  may be evaluated by a formula  $\sigma_{\text{th}} = \rho_0 c_0^2 / (4b)$ , where  $\rho_0$  is the normal density of the substance,  $c_0$  and  $b$  are the coefficients the Hugoniot  $D = c_0 + bU$  [2],  $D$  is the shock velocity,  $U$  is the particle velocity. According to data [3],  $c_0 = 3$  km/s,  $b = 1.35$  for graphite MF-307. As a result, the ultimate tensile strength of MF-307 is evaluated not higher than 3.3 GPa. Analogous value in the case of graphite PG-5 is equal to 2.7 GPa.

The study of dynamic mechanical strength of graphite is interesting because, to date, no published data on physical properties of graphite at negative pressures are available. It is also interesting to compare the data on the dynamic strength of graphite with similar data for other allotropic modification of carbon—diamond.

## 2. Experimental conditions

The experiments were carried out at two laser systems operating on neodymium glass: “Kamerton-T” and PHELIX. The basic laser radiation is converted into the second harmonic with a wavelength of 0.53  $\mu\text{m}$ . The energy of the laser pulse reaching a value of 1 J (in the first case), and 120 J (in the second case). The laser beam was focused on the target over a spot with the diameter of 0.4 to 1.4 mm. The maximum value of the flux density of the laser radiation in the focus area reached  $1.6 \times 10^{13}$  W/cm<sup>2</sup> and the ablation pressure—0.6 TPa. Details of the experiments are shown in table 1. The scheme of the experiments is shown in figure 1.

The morphology of the front and back surfaces of samples after the laser irradiation was investigated using a scanning electron microscope (SEM). Relief of fracture zone and the depth of the crater on both surfaces of the samples were measured by optical metallographic microscope MF-8 with an accuracy of 1  $\mu\text{m}$ .

Structure of matter on the irradiated and spallation surfaces of samples is analyzed by Raman scattering with a confocal spectrometer HR800-180 (Horiba Jobin Yvon) with a spectral resolution of 0.5 cm<sup>-1</sup>. For Raman excitation, two types of lasers were used: He-Ne laser with a wavelength of 632.8 nm (20 mW) and Nd-YAG laser with a wavelength of 532 nm (40 mW).

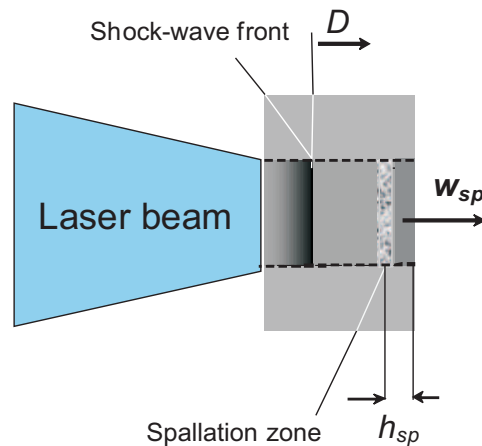


**Figure 1.** The experimental setup:  $D$ —the velocity of the shock front,  $h_{sp}$  and  $w_{sp}$ —thickness and velocity of the spall plate, respectively.

In both cases, the spatial resolution is about  $2\ \mu\text{m}$ .

### 3. The method of determining the spall strength and strain rate

For determining values of the spall strength  $\sigma_*$  and the strain rate  $\dot{V}/V_0$  of matter (where  $V_0$  is the initial value of the specific volume,  $\dot{V} = dV/dt$  is the rate of its changing upon time), the spall cavity depth  $h_{sp}$  was measured after the action on the target, and mathematical modeling of shock-wave flow at the measured spall coordinate was carried out [4, 5]. For calculating the values of  $\sigma_*$  and  $\dot{V}/V_0$ , a numerical code was used, which is created by the Courant–Isacson–Rees scheme on the basis of the hydrodynamic equations [6]. In the code, a wide-range equation-of-state model [7, 8] was used for graphite. It was supposed that the time profile of the ablation pressure pulse on the facial surface of the target follows the profile of the laser radiation pulse. A relation between the amplitude of the ablation pressure pulse  $P_a$  (TPa) and the maximal intensity of the laser radiation  $I_l$  (TW/cm<sup>2</sup>) was specified by semiempirical formulas [9]:

$$P_a = \begin{cases} 1.2(10^{-2}I_l)^{2/3}\lambda^{-2/3}[A/(2Z)]^{3/16} & \text{at } I_l \geq 4.3\ \text{TW/cm}^2, \\ 1.4(10^{-2}I_l)^{7/9}\lambda^{-3/4} & \text{at } I_l < 4.3\ \text{TW/cm}^2, \end{cases} \quad (1)$$

where  $\lambda$  is the wavelength of laser radiation ( $\mu\text{m}$ ),  $A$  is the atomic weight,  $Z$  is the atomic number of the target substance.

In the experiments, the only values of the laser pulse intensity  $I_l$  were fixed, at which the spall occurred. The minimal (negative) values of the pressure calculated at the measured position of the spall plane are recognized as the values of the spall strength  $\sigma_* = |P_{\min}|$  (tensile strength). The strain rate was determined by calculation of temporal dependence of the density  $\rho(t)$  and its derivative with respect to time,  $\dot{V}/V_0 = |\dot{\rho}/\rho_0|$ .

## 4. Obtained results

### 4.1. The morphology of the surface spallation target

Figure 2 (on top) shows SEM images with a different magnification the back (spall) side of the sample 1 after shock-wave action. In the experiment 6, spallation happened, but the spall plate was not separated from the target and so preserved for further analysis. Optical image of the plate is shown in figure 2 (below). The plate has a quasi-conical shape with an apex angle  $120^\circ$ . This is a significant difference from the case of metals where spall plates are flat [10].

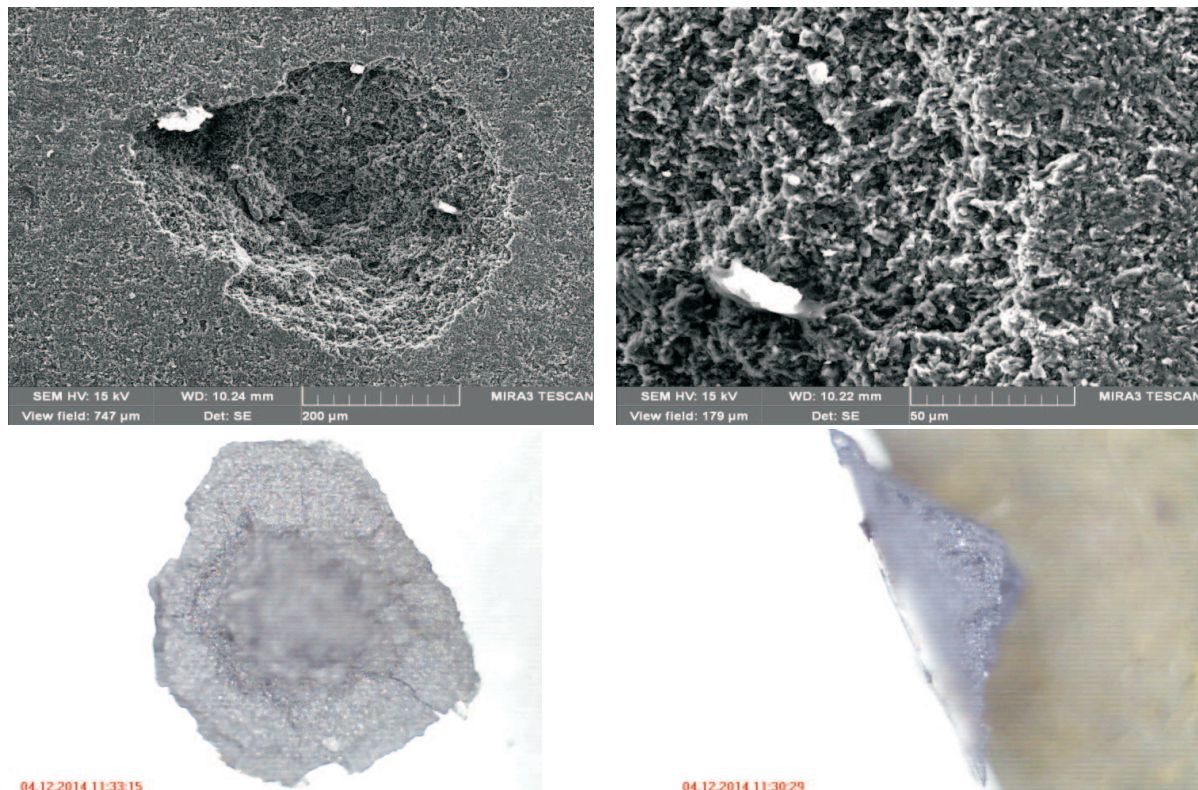


**Figure 2.** On top—SEM images with different magnification rear (spall) side of the sample 1 after shock-wave action. Below—the optical image on the inside (left) and from one side (right) of the spall plate preserved in shot 6 (the angle at the vertex of the spall plate— $120^\circ$ ).

#### 4.2. Graphite structure on the facial and back surfaces of targets

The main crystalline phase of graphite MF-307 (samples 1–3) is graphite with hexagonal structure. The material, together with crystalline phase also contains a small portion of amorphous components. Samples of graphite PG-5 (samples 4–6) is a polycrystalline graphite grains with size  $\approx 20$  nm.

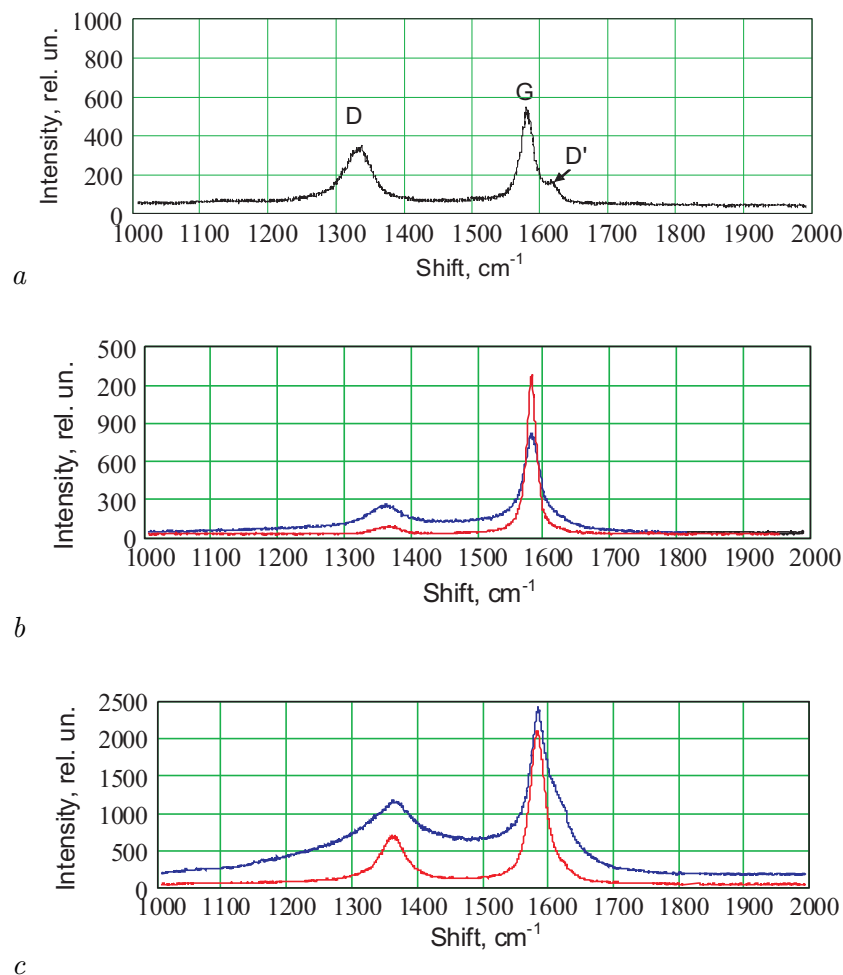
Results of Raman spectroscopy of graphite PG-5 (samples 4 and 5) after laser action are shown in figure 3 and table 2. Figure 3a shows the Raman spectrum of the initial sample of graphite PG-5. Figure 3b shows the Raman spectra obtained within irradiated spot of the target surface from experiment 4. The lower and top curves correspond to the center and the edge of the ablation crater. Based on the analysis of the obtained spectra, one can make the following conclusions. In the crater center, matter is the graphite with a perfect structure resulting from recrystallization of the source material. At the edge of the crater, matter is likely to have disordered graphite structure that is characteristic to turbostratic carbon form, which is close to the soot structure.

Figure 3c illustrates a comparison of Raman spectra recorded in the experiment 5 within the laser impact area on the front surface (upper curve) and in the region of the crater on the back surface of the target (the lower curve). Raman spectrum in the spallation area indicates a very good recrystallized structure of graphite with a small disordering and better crystallinity in comparison with the original material.

G-line of the spectrum corresponds to the position of the Raman line of the monocrystalline graphite, and D-line appears due to the finite size of the crystallites, disordering and possible defects of the sample, D'-line accompanies usually the D-line appearance.

**Table 2.** Characteristics of the Raman spectra of graphite PG-5 samples before (original) and after laser irradiation:  $I_D/I_G$ —the ratio of the intensities of the spectral lines D and G, FWHM(G) and FWHM(D)—the full widths at half of the maximum intensity of the lines D and G, respectively.

Sample	$I_D/I_G$	FWHM(G), $\text{cm}^{-1}$	FWHM(D), $\text{cm}^{-1}$
Original graphite	0.59	24.5	47.8
No. 4, the irradiated area edge	0.42	51.4	100
No. 4, the irradiated area center	0.31	27.7	51.1
No. 5, the irradiated area center	0.25	32.1	89.9
No. 5, spallation zone	0.12	21.4	50



**Figure 3.** Raman spectra of the graphite PG-5 target: *a*—outside the area of laser irradiation; *b*—in the irradiated area after shot 4 (graph on top corresponds to the area edge, graph below—the area center); *c*—in the irradiated area after shot 5 (graph on top) and in the spallation crater on the back surface of the target after shot 5 (graph below).

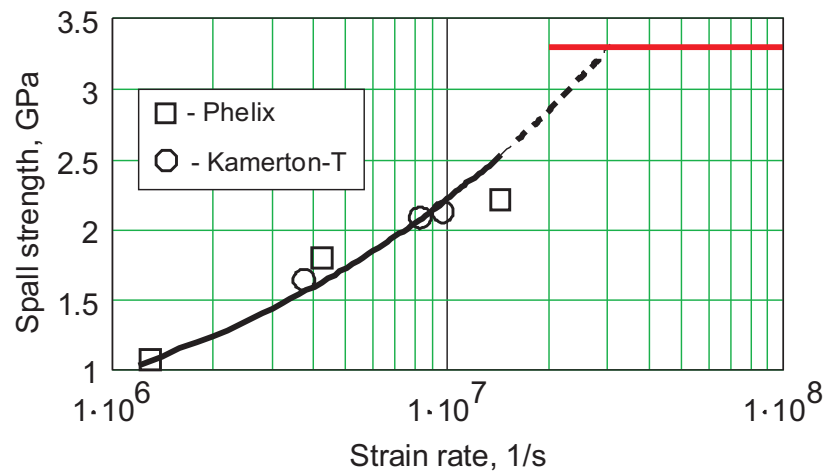


**Figure 4.** The dependence of spall strength of graphite upon the strain rate.

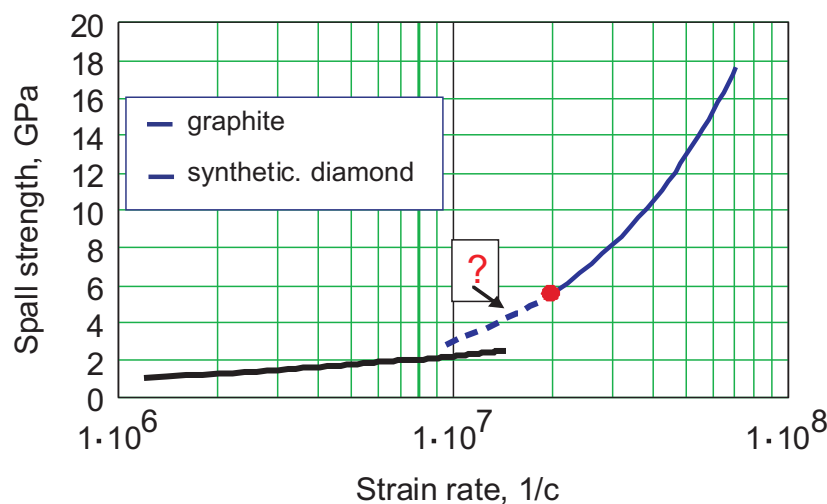


**Figure 5.** Comparison of the dynamic strength data for graphite (this work) and synthetic diamond [11,12]. Dashed line is a continuation of the experimental curve for the diamond to the strain rates below the studied range [11,12] boundary (that is marked).

#### 4.3. The dependence of spall strength for graphite samples upon strain rate

Experimentally obtained spall strength  $\sigma_*$  of graphite is shown in figure 4 as a function of the strain rate  $\dot{V}/V_0$ . The data approximated with least squares method are expressed by means of the curve described as  $\sigma_* = 6.7 \times 10^{-2}(\dot{V}/V_0)^{0.36}$ , where  $\sigma_*$  is measured in units of GPa,  $\dot{V}/V_0$ —1/s.

Inaccuracies of determining the spall strength and the strain rate are associated primarily with a finite width of the spall area. Analysis of the experimental data and calculation results shows that the maximum errors of determining the values of the spall strength and strain rate are 5 and 38%, respectively. In the experiment, the magnitude of the spall strength  $\sigma_* \approx 2.1$  GPa, which is 64% of the theoretical ultimate tensile strength of the graphite calculated according to the equation of state [7], 3.27 GPa.

Figure 5 shows a comparison of the data obtained for the graphite with those for the synthetic diamond [11, 12]. One can see that, at strain rate  $\approx 1 \times 10^7 \text{ s}^{-1}$ , the spall strength of graphite and diamond may probably be equal. However, verification of such a probability requires an additional measurement of the spall strength of the diamond at strain rates of  $(1\text{--}1.2) \times 10^7 \text{ s}^{-1}$ .

## 5. Conclusion

Thus, the data on the dynamic tensile strength of the graphite at strain rates from  $10^6$  to  $10^7 \text{ s}^{-1}$  are obtained for the first time. Attained maximal value of the spall strength of graphite  $\sigma_* \approx 2.1 \text{ GPa}$  is 64% of theoretical ultimate tensile strength. Obtained Raman spectra indicate changes of the crystalline structure of original graphite materials, as on the irradiated surface, as in the spallation zone on the backside of the target.

## Acknowledgments

Authors are grateful to A I Savvatimsky for providing with the samples of graphite MF-307 and R O Gavrilin, S M Savin, A V Bogdanov, V A Panyushkin, A V Bakhmutova, A P Kuznetsov and K L Gubskii for help in the experiments.

This work was financially supported by grants of the Russian Foundation for Basic Research (No. 12-02-00625, 12-02-00746, 13-02-91057, 14-08-00967 and 14-29-06099) and the President of the Russian Federation (No. NSH-451.2014.2 and NSH-6614.2014.2), as well as the programs of the Presidium RAS (No. 13P “Extreme light fields and their applications” and 2P “Matter at high energy density”). We are also grateful for the support by the FP7 EuCARD-2 grant No. 312453 and the Federal Ministry of Education and Research of Germany.

## References

- [1] Zel'dovich Y B and Raizer Y P 1967 *Physics of Shock Waves and High-Temperature Hydrodynamic Phenomena* (New York: Academic Press)
- [2] Kanel' G I, Razorenov S V, Utkin A V and Fortov V E 1996 *Shock-Wave Phenomena in Condensed Media* (Moscow: Yanus-K)
- [3] Levashov P R, Khishchenko K V, Lomonosov I V and Fortov V E 2004 *AIP Conf. Proc.* **706** 87–90 URL <http://www.ihed.ras.ru/rusbank/>, <http://www.ficp.ac.ru/rusbank/>
- [4] McQueen R G and March D 1962 *J. Appl. Phys.* **33** 654–665
- [5] Batani D, Vovchenko V I, Kanel G I, Kilpio A V, Krasnyuk I K, Lomonosov I V, Pashinin P P, Semenov A Y, Fortov V E and Shashkov E V 2003 *Dokl. Phys.* **48** 123–125
- [6] Kulikovskiy A G, Pogorelov N V and Semenov A Y 2012 *Mathematical Problems of Numerical Solving Hyperbolic Systems of Equations* (Moscow: FIZMATLIT)
- [7] Lomonosov I V, Fortov V E and Khishchenko K V 1995 *Khim. Fizika* **14** 51–57
- [8] Khishchenko K V 2015 *J. Phys.: Conf. Series* This issue (Preprint [arXiv:1510.00763](https://arxiv.org/abs/1510.00763))
- [9] Vovchenko V I, Krasnyuk I K, Pashinin P P and Semenov A Y 1994 *Dokl. Akad. Nauk* **338** 322–324
- [10] Abrosimov S A, Bazhulin A P, Voronov V V, Geras'kin A A, Krasnyuk I K, Pashinin P P, Semenov A Y, Stuchebryukhov I A, Khishchenko K V and Fortov V E 2013 *Quantum Electron.* **43** 246–251
- [11] Abrosimov S A, Bazhulin A P, Bol'shakov A P, Konov V I, Krasnyuk I K, Pashinin P P, Ral'chenko V G, Semenov A Y, Sovyk D N, Stuchebryukhov I A, Fortov V E, Khishchenko K V and Khomich A A 2014 *Quantum Electron.* **44** 530–534
- [12] Abrosimov S A, Bazhulin A P, Bolshakov A P, Konov V I, Krasiuk I K, Pashinin P P, Ralchenko V G, Semenov A Y, Sovyk D N, Stuchebryukhov I A, Fortov V E, Khishchenko K V and Khomich A A 2015 *J. Appl. Mech. Tech. Phys.* **56** 143–149